Impact of cyclic freezing on LNAPL movement in a single fracture

Olumide Iwakun & David Sego
Department of Civil and Environmental Engineering - University of Alberta, Edmonton, Alberta, Canada
Kevin Biggar
BGC Engineering Inc., Edmonton, Alberta, Canada

ABSTRACT

Porous media including fractured bedrock in cold regions undergo cyclic freezing and thawing due to seasonal variation in temperature. Spilled fuel in such environment is difficult to cleanup because of inadequate understanding of its subsurface behavior. In this study, a freezing cell consisting of two parallel glass plates with emplaced glass beads was constructed in the laboratory to simulate a bedrock fracture and determine the impact of cyclic freezing on LNAPL movement. The test procedure involved introduction of LNAPL atop the freezing cell that contained water mixed with fluoroscein dye, in a top-down freezing test. LNAPL migration was observed and measured using a high-resolution digital camera with time-lapse photography. Both diesel and soluble oil were used for the experiment. Tests with soluble oil involved thorough mixing at 12.5% volume ratio with the fluoroscein-water in the freezing cell. The results showed upward mobility of free phase diesel under cyclic freezing, and downward progressive expulsion of the soluble oil ahead of freezing front during freezing. The results corroborated literature findings on organic solute expulsion ahead of freezing front, and provided insight into the behavior of trapped LNAPL below the water table when subjected to freezing conditions.

Résumé

Les médias poreux comprenant la roche en place rompue dans des régions froides subissent congélation cyclique et dégel dû à la variation saisonnière de la température. Le combustible renversé dans un tel environnement est difficile nettoyer en raison de arrangement insatisfaisant de son comportement à fleur de terre. Dans cette étude, une cellule de congélation se composant de deux plaques de verre parallèles avec les perles en place a été construite dans le laboratoire pour simuler une fracture de roche en place et pour déterminer l'impact de la congélation cyclique sur le mouvement de LNAPL. La procédure d'essais a comporté l'introduction de LNAPL placé sur la cellule de congélation qui a contenu de l'eau mélangée au colorant de fluoroscein, dans un essai de gélivité de haut en bas. La migration de LNAPL a été observée et mesurée utilisant un appareil photo numérique à haute résolution avec la photographie de temps-faute. De l'huile diesel et soluble ont été employées pour l'expérience. Les essais avec de l'huile soluble ont comporté le mélange complet au rapport de 12.5% volumes à la fluoroscein-eau dans la cellule de congélation. Les résultats ont montré la mobilité ascendante du diesel libre de phase sous la congélation cyclique, et l'expulsion progressive de haut en bas d'huile soluble en avant d'avant de congélation pendant la congélation. Les résultats ont corroboré des résultats de littérature sur l'expulsion organique de corps dissous en avant de l'avant de congélation, et si l'aperçu du comportement de LNAPL emprisonné au-dessous de la nappe phréatique une fois soumis à la congélation conditionne.

1 INTRODUCTION

Successful remediation of spilled fuel in porous media including fractured bedrock requires adequate understanding of its subsurface behavior. Most spilled fuels (i.e., gasoline and diesel) are subsets of light nonaqueous phase liquid (LNAPL) because they are less dense than water and mostly immiscible with it. In temperate regions, the behavior of spilled fuel is well-documented in the literature. However, in cold regions overlapping permafrost environments, subsurface behavior of spilled fuel is an ongoing research area.

Permafrost is often viewed as a barrier to contaminant migration in cold region, which has often contributed to improper environmental practices involving spilled fuel (Barnes and Chuvilin, 2009). Studies have shown that ice or completely ice-saturated frozen soil without defects have very low permeability in the order of 10^{-15} cm^2, and are mostly impervious. This formed the basis for the development and use of frozen core barrier for contaminant mitigation. A study by Anderson et al. (1996) on such barrier's resistance to ice erosion by liquid contaminant showed that minimization of ice erosion requires full ice saturation and barrier temperature below the freezing point depression of the contaminant. However, in ice-saturated frozen soil, there is a natural propensity for microcracks development, especially at temperatures below freezing (Yershov et al., 1988) because frozen ground is a spatially inhomogeneous system (Frolov, 1982).

Laboratory experiment by Biggar and Neufeld (1996) on vertical migration of diesel into columns of saturated silty-sand subjected to freeze-thaw cycles showed no contamination in the permanently frozen soil layer at depth after eight cycles of freeze-thaw. The diesel contamination was limited to the saturated soil up to the thaw depth. Thus, they postulated that the contaminant movement into the saturated soil was due to migration in fissures induced during freezing However, site investigations of fuel migration at two different fuel-contaminated sites in the Canadian Arctic by Biggar et al. (1998) found significant contamination below the permafrost table. They postulated that gravity drainage along fissures induced by thermal contraction, or gravity drainage via interconnected air voids accounted for this movement. Thus, permafrost may not be an effective barrier to contaminant propagation.

Laboratory investigation of factors affecting oil migration in frozen ground by Chuvilin et al. (2001) showed that oil penetration decreased with increasing ice saturation but increased with decreasing hardening temperature of the oil. Components of oil were observed even in wholly ice-saturated soil, corroborating the work of Biggar et al. (1998). Later work by Chuvilin and Miklyaeva (2003) suggested that capillary transfer via micropores may be responsible for the oil penetration. Chuvilin et al. (2001) also showed that surface spreadability increased with increasing ice saturation and oil hardening temperature but decreased from sand to clay to ice as a result of increasing wetting angle on the mineral surfaces respectively. Laboratory experiment by Barnes and Wolf (2008) on the effects of pore-ice on spreadability and penetration of petroleum products in coarse grained soils showed that ice content increased lateral migration of petroleum due to the formation of dead end pores by ice especially in the vadose zone, thereby creating irregular preferential flow paths resulting in deeper contaminant penetration.

The nucleation process that occurred during ice formation is known to cause rejection and concentration of solutes in the unfrozen water (Konrad and Seto, 1991; Tumeo and Davidson, 1993; and Chuvilin et al., 2001). This process is commonly referred to as solute exclusion or rejection in freezing experiments and hydrocarbon exclusion when petroleum products are involved. Barnes and Chuvilin (2009) referred to this process as cryogenic expulsion, and related it to separation of more mobile components from petroleum. In this study, the term “cryogenic expulsion”, is adopted. Different studies have shown that cryogenic expulsion is enhanced at lower freezing rates (Konrad and McCammon, 1990; Konrad and Seto, 1991; Panday and Corapcioglu, 1991), however, the phenomenon had been observed at higher freezing rates (Ershov et al., 1992). In a top-down freezing experiment conducted by Konrad and Seto (1991) on a partially saturated clay sample contaminated with miscible organic solvent (propanol), there was an increase in solvent concentrations in front of advancing freezing front. Other studies conducted in the laboratory corroborated such observation (Chuvilin et al., 2001; Tumeo and Davidson, 1993; Panday and Corapcioglu, 1991). According to Wilson and Mackay (1987), freezing can cause oil to weather, which may lead to increased density and viscosity, thereby enhancing downward pull potential but decreased fluid’s mobility.

Fluctuations of groundwater table have been shown to enhance LNAPL entrapment and remobilization in the formation (Lenhard et al., 1993: Catalan and Dullien, 1995; and Dobson et al., 2007). Aral and Lao (2002) developed numerical models to mimic this behavior. Dobson et al. (2007) further showed that water table fluctuation enhances biodegradation and dissolution of LNAPL components, and increases its migration down-gradient. Ryan and Dhir (1993) performed laboratory column tests using glass bead packs of various sizes to investigate the effect of particle diameter on LNAPL entrapment due to a slowly rising water table. The results showed enhanced LNAPL entrapment for pre-wetted particles but insignificant effect for particle sizes less than 710 µm with an average residual saturation of 11%. Larger particles showed significant reduction on residual saturation.

Iwakun et al. (2008b) correlated measured LNAPL thickness in a monitoring well (MW) at a fuel-contaminated site in Canadian North with both the groundwater elevation and the thermal profile at the MW’s location. The study showed significant inverse correlation of the LNAPL thickness with both the thermal profile and the groundwater elevation. Furthermore, increased LNAPL accumulation in the MW in early winter corresponded to decreased groundwater elevation and vice-versa in early spring when the groundwater table was elevated. There was no significant recharge of LNAPL in the MWs following product recovery test in the winter (Iwakun and Biggar, 2007), inferring the mechanisms enhancing LNAPL accumulation at the site are not continuous. Further investigations at the site showed that LNAPL contamination is generally limited to the upper seven meters of the subsurface, which consists of 0 – 4.6 m of overburden soil underlain by fractured bedrock (Iwakun et al., 2010). From the site characterization efforts at the site, Iwakun et al. (2008b) suggested that freezing-induced capillary drainage, gravity drainage due to groundwater table fluctuation, and thermal induced processes are mechanisms controlling LNAPL migration and accumulation in MWs at the site. Thus, this study was designed to complement the previous field work by Iwakun et al. (2010) and evaluate the hypothesis that freezing induced displacement may play a secondary role in mobilizing contaminant at the site.

Consequent to discussions above, a freezing cell made of two parallel glass plates representing a fracture was constructed to evaluate the influence of freezing-induced displacement and freeze-thaw cycles on LNAPL mobility, and the effect of freezing on dissolved oil components in water.

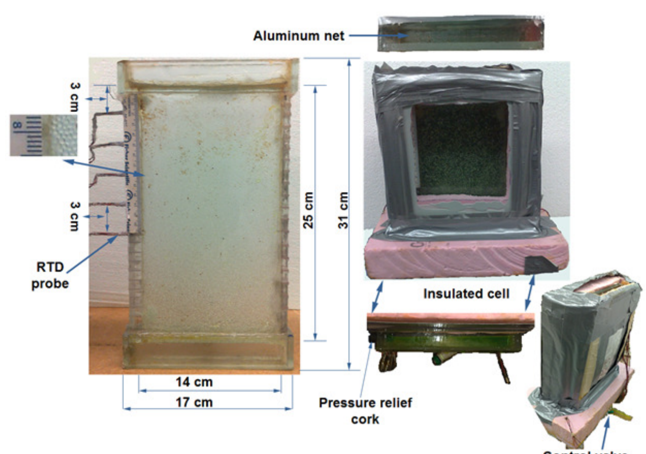

Figure 1 Fabricated freezing cell used for the experiment.

The method used in this study was a modification of those used by various authors to investigate pore-scale behavior of contaminant in freezing porous media (Niven and Singh, 2008; Barnes and Wolfe, 2008; and Arenson and Sego, 2006).

2 METHODOLOGY

Materials: Process control equipment (RTD regulator; range ±199.9oC, MODEL 4201APC2-T, omega); two glycol baths (LAUDA BRINKMANN, ecoline RE 120); digital camera (canon SLR 1000D); two computers; freezing cell; Agilent data acquisition unit; diesel; soluble oil; fluorescein; two fluorescent light tube-units; air bag heater; water bath; insulated enclosures; RTD probes; copper freezing plates; and weights were used.

2.1 Freezing cell

The freezing cell is constructed from Perspex glass as shown in Figure 1. It consists of sealed parallel glass plates to mimic a fracture interspaced at 1 mm (1000 µm). The initial intent was to roughen the internal surfaces of the glasses but due to visibility issues, glass beads were placed within the fracture. The objective of placing beads within the freezing cell is to enable entrapment of LNAPL within the water column. The dimensions of the freezing cell are included in Figure 1. Five detached RTD probes were fitted to one of the edges of the cell to monitor the thermal profile during the test. A control valve with pressure relief cork is fitted to the base of the cell. The control valve is used to moderate water filling while the pressure relief cork is to prevent cracking of the apparatus due to volume change of ice. The tube connecting the control valve to the cell is made of expandable rubber to accommodate for displaced water during top-down freezing.

The top of the cell is uncovered with an emplaced aluminum net to prevent the beads from falling and enhance heat dissipation. The apparatus was checked for leaks prior to testing and the attached RTD probed were calibrated before attachment to the cell using silicone glue.

The cell is insulated as shown in Figure 1 prior to the testing. The insulation consists of foam with a glass window as shown in Figure 1. The glass window provides the needed opening for photographing during test. The whole assembly is then placed inside a water bath in an environmental chamber, which is made up of a deep freezer with external temperature control equipment.

Beads emplacement was done by first setting the required fracture width at both ends of the parallel glass plates and sealing the sides with silicone-laminated glass and the base with a porous filter. The beads were cleaned with hydrofluoric acid before placement into the created aperture. It should be noted that the beads were not of uniform size and shapes. Thus, during placement, some beads get stuck and had to be pushed down using thin wire gauze. Non-uniformity of the beads geometry led to slight overlapping of some beads within the cell. Porous filter-glass was used between the RTD ports and the beaded filled-annulus of the cell.

2.2 Setup

Steps taken in setting up the experimental system can be divided into three, namely, cell-filling, cell-placement, and testing. Prior to these steps, preliminary setup tasks included:

- Placement of the digital camera in an insulating chamber with an air-bag heater. The front face of the insulating chamber consists of a 14 cm X 14 cm glass window for picture taking. Inside of the insulting chamber is coated black to minimize light reflection. The camera runs off AC-battery power source, and the lens is manually focussed to achieve highest picture quality.
- Positioning of water bath consisting of glycol-operated heating element with an open water interface (for sitting the freezing cell) in the environmental chamber.
- Placement of stand inside the environmental chamber to secure the thermal freezing plate.
- Provision of secondary lighting system inside the environmental chamber. The provided lighting system consists of two low heat generating fluorescent units.
- Elevation alignment of the camera and the emplaced bath in the environmental chamber.
- Addition of fluorescein to the water for use in the experiment.
- Connection of the camera and external Agilent data acquisition units to two different computers for data logging. Two computers were used in order to optimize system resources.

2.3 Cell-infilling

Infilling of the cell was carried out from bottom up at 0.5 mL/min via gravity displacement. An external reservoir consisting of a graduated cylinder containing a fluorescein-water mixture with a fitted control valve was connected to the bottom control valve of the freezing cell via rubber tubing. Both valves were opened to achieve the desired flow rate. The cell was tilted during initial infilling with the pressure relief cork removed to allow escape of air and prevent formation of air-bubbles within the cell. When all the air at the base of the cell was displaced, the pressure relief cork was inserted, the cell was straightened up and filled until the upper open chamber is a quarter full.

To create a mixture of diesel and water, diesel was introduced at the open-end of the cell atop the fluorescein-water with the control valves of both the cell and the reservoir kept open. The reservoir is then lowered to allow drainage of the diesel into the cell. This is akin to fluctuation of the water table in the field. Additional water was introduced via the top in conjunction with lowering the reservoir until LNAPL entrapment occurred. Then, the valves were closed and the system was allowed to equilibrate, which often involves some vertical movement of un-trapped LNAPL to the top of the cell.

In tests involving soluble oil, the soluble oil is mixed with the fluorescein-water mixture in the external reservoir, and used in filling the cell as discussed previously by gravity displacement. The properties of the soluble oil and diesel used for the experiment are given in Table 1.

Table 1 Characteristics of the fuel and soluble oil used for the experiment.

Parameter	Diesel	Mobilcut-102	BAND-ADE® Sawing fluid
Solubility in water (20°C)	Insoluble (< 40 mg/L)	100%	100%
Specific gravity (25°C)	0.8171	0.89	1.02
Appearance	Colorless	Translucent amber	Translucent amber
Pour point (°C) or hardening temperature	-30	-6	-6
Dynamic viscosity (cp)	4 @ 0°C 2 @ 15°C	30 @ 40°C	9.5 @ 25°C
Surface tension (mN/m)	27.7 @ 0°C 23.8 @ 25°C		

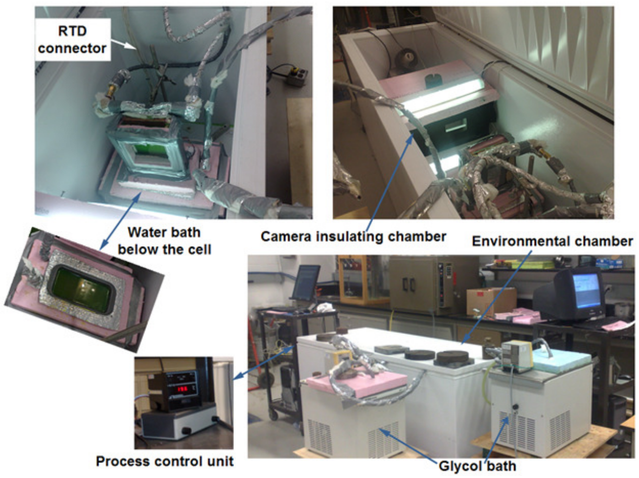

Figure 2 Setup of the laboratory system showing the freezing cell placement in the environmental chamber.

2.4 Cell-placement

After filling the cell with the fluid(s) of interest, the detached RTD probes at the side of the freezing cell was reattached to the Agilent data acquisition unit, which was connected to the computer. The freezing-cell assembly is then placed inside the environmental chamber with its base sitting in the bath as shown in Figure 2.

Freezing plate was attached to the top of the cell and in contact with the open section of the cell. The freezing plate was firmly secured to the stand inside the environmental chamber. The fluorescent lights were turned on and arranged at the top and bottom of the windowed area of the camera chamber to achieve optimum picture quality. The camera was turned on and weights ranging from 10 to 20 kg were placed atop the environmental chamber for proper sealing (Figure 2).

2.5 Testing

After placement of the freezing cell and closure of the environmental chamber, the two glycol baths were turned on to maintain the test temperature. One glycol bath controls the temperature of the lower bath while the other controls the temperature of the freezing place. For this test, the temperature of the glycol bath controlling the lower bath was set to +10°C and that of the freezing plate was set to -10°C. For the control experiment, the temperatures were varied to study heat propagation through the test cell. The temperature inside the environmental chamber was set to -2.5°C using the external temperature control unit.

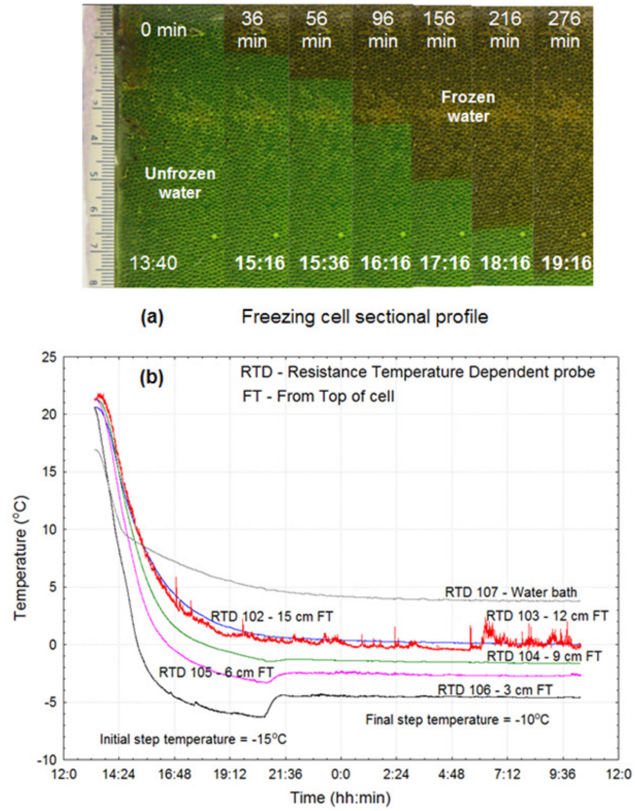

Figure 3 Thermal propagation for the control experiment, (a) Snapshots of freezing progression in the cell; (b) temperature profile.

However, another RTD probe placed inside the environmental chamber showed that the temperature remained -3 ±1°C. Then the data loggers for both the camera and the RTD Agilent data acquisition unit were turned on.

2.5 Test series

Three series were involved in the evaluation of the study objectives. The first series is the control phase, aimed at assessing the system performance. Only fluorescein-water mixture was used in this series, and freezing was top-down. The rate of freezing and frost penetration under different thermal gradient were measured and used to benchmark later tests. The freezing rate was calculated using:

$$\frac{dT}{dt} = \frac{dT}{dx} \times \frac{dx}{dt} \quad \left| \begin{array}{l} \frac{dT}{dx} \rightarrow \textit{Thermal gradient} \\ \\ \frac{dx}{dt} \rightarrow \textit{Rate of frost penetration} \end{array} \right. \qquad [1]$$

The second series was aimed at evaluating the influence of freeze-thaw on LNAPL and emulsified oil movement. This series involved the use of diesel fuel and soluble oil. It should be noted that the diesel fuel used for this test was not colored because coloring caused it to adhere to the glass beads. The last series of the test involved evaluating the influence of freezing from the second test series on the development of micro-fissures. In the series, the step temperature was varied from -10°C to +1°C, while the base and ambient temperatures of the environmental chamber were kept constant. The upper step temperature range during thaw was limited to +1°C because sudden thermal changes in the temperature caused moisture deposition on the surface of the freezing cell, leading to blurred photographic images.

3 RESULTS AND DISCUSSION

Figure 3 shows the thermal propagation for the control experiment. The rate of frost penetration was initially rapid until a steady state was reached after about 19 hours (Figure 4a). The average cooling rate of the system was 1.4°C/day at steady state thermal gradient and the frost front continued to move downward at a decreasing rate. The cooling and frost penetration rate were more than an order of magnitude greater than that observed in the field (Figure 4b), but within range of values reported in the literature. From Figure 3a, freezing caused the fluorescein-water to change color from blue to grey. During the first freezing test, rearrangement of the glass beads occurred within the cell as the freezing front propagated downward. This behavior was expected because freezing was known to enhance consolidation in porous media. Subsequent freezing does not result in particle rearrangement during freezing because optimum compaction of the beads was achieved during the first freezing. One of the four pins in RTD 103 attached to the side of the cell was accidentally cut and replaced before placement in the environmental chamber. The RTD 103 was not recalibrated before placement because doing so would require dismantling the apparatus, which will take additional days before system set-up. Thus, readings from RTD 103 had a lot of noise. Thus, the readings from this RTD were excluded from thermal profile of subsequent tests.

The results for the second test series involving diesel fuel are summarized in Figures 5 and 6. There was delayed frost penetration into the cell due to lower thermal conductivity of the diesel fuel compared to water. The cooling rate was 0.7°C/day less than that of the control experiment during the first test series to establish steady state thermal gradient (Figure 5). At the onset of freezing, rearrangement of trapped LNAPL bubbled within the cell resulted into upward displacement of the LNAPL (Figure 6). Thus, as freezing progressed, no downward movement of the mobile LNAPL was observed.

Instead, freezing caused upward remobilization of the trapped but mobile LNAPL (Figure 6). Further along the cell, there were instances where the expanding ice rearranged isolated blobs of LNAPL. The displacement resulting from this rearrangement was small and difficult to quantify. The reason for this may be that the forces generated by the expanding ice was not mobilized before freezing-induced suction and buoyant forces on the were established. From the general equation at the freezing front developed from the Clausius-Clapeyron equation (eqn. 2), suction is generated at the freezing front. Combination of this with upthrust on the LNAPL blob and capillary action favors upward mobility of the LNAPL as freezing is initiated.

$$P_w = \frac{L}{V_w}\ln\frac{T^*}{T_o} + \frac{V_i}{V_w}P_i \quad (dG_{ice} = dG_{water}\ at\ freezing\ front)$$

$$\Delta P = \left(P_w - \frac{V_i}{V_w}P_i\right) = \frac{L}{V_w}\ln\frac{T^*}{T_o} = \left.\frac{L(T^* - T_o)}{V_w T_o}\right|_{T^* \to T_o}$$

$$\therefore \Delta P = \frac{L\Delta T}{V_w T} \qquad [2]$$

Where, P, G, V, L, and T in equation 2 stand for pressure, Gibbs' free energy, specific volume, latent heat, and temperature. Subscript w and I indicate water and ice respectively. T* stands for temperature at which both water and ice co-exists (i.e., $T^* < 0$°C), and T_o stands for reference freezing temperature of pure water (= 0°C or 273 K).

In a bottom-up freezing tests, Niven and Singh (2008) postulated that the freezing-induced ice pressure on LNAPL accounted for its upward mobilization and ganglia rupture. This freezing-induced pressure was estimated to be in the order of mega Pascal (MPa) if fully mobilized and dependent on the LNAPL saturation. However, there was no downward LNAPL mobilization in the top-down freezing tests conducted in this study.

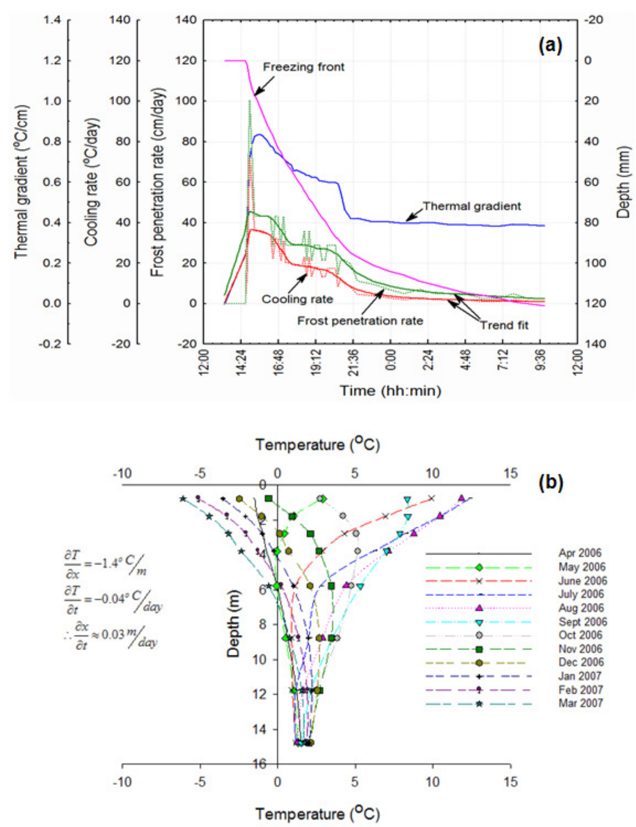

Figure 4 Comparison of laboratory and field thermal profile: (a) Frost penetration profile for the control experiment, and (b) sample of temperature profile in MW 12 at the Colomac mine site (Iwakun et al. 2008b).

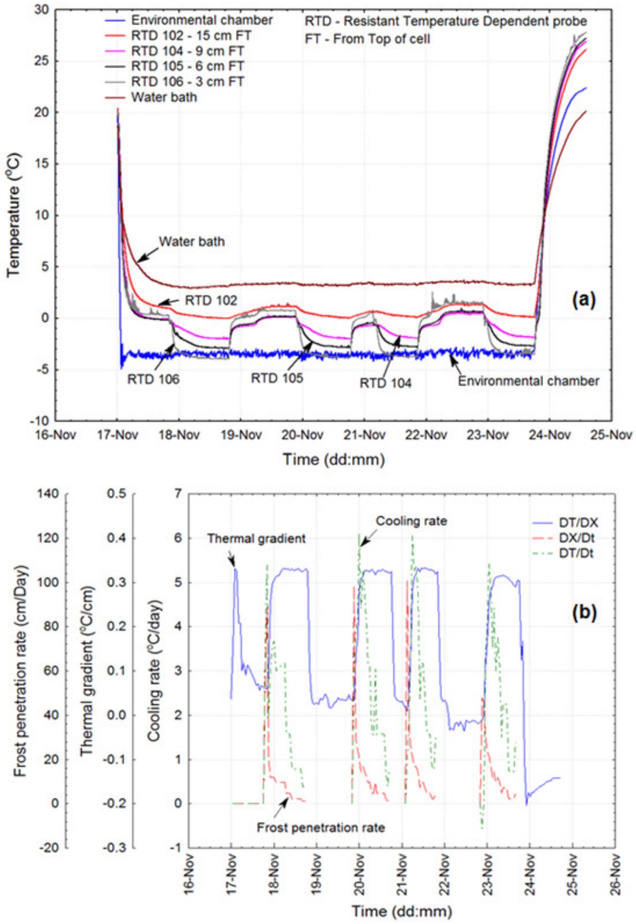

Figure 5 Freezing-test results using diesel subjected to freeze-thaw cycles. (a) Temperature profile; (b) profile for thermal propagation rates.

The observed displacement that took place after cyclic freezing in this study was opposite to the direction of freezing. It is difficult to quantify lateral remobilization in these tests, thus the cumulative upward LNAPL displacement was used and plotted as shown in Figure 6b. The results showed that LNAPL remobilization and displacement took place at the onset of freezing and during thawing. There was little displacement after the second thaw (2-T) and third freezing (3-F) cycles because insufficient time was allowed for pressure dissipation and ice melting within the cell (Figure 6a). During freezing, the LNAPL within the cell remained unfrozen as the surrounding water changed phase. The expansion of the frozen water surrounding the LNAPL may induce pressure in the LNAPL. Thus, on thawing, the pressure relief coupled with the LNAPL's buoyant nature enhanced its upward mobility. Moreover, this test showed that freezing induced displacement is a viable mechanism for LNAPL transport; however, further studies are needed to evaluate conditions that favour blobs of LNAPL being displaced forward of freezing front due to ice expansion as stipulated by Barnes et al. (2004).

It is well established in the literature that decreasing temperature causes increase in surface tension and capillarity in a porous media (Grant and Bachmann, 2002).

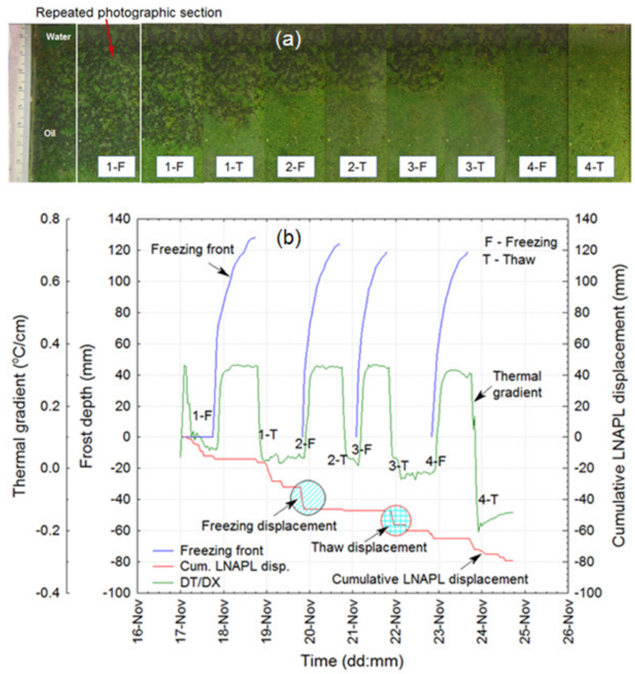

Figure 6 Frost penetration profile for freezing test with diesel (Figure 5): (a) Snapshots of upward displacement of diesel at the start of freezing and during thawing; (b) Plots of cumulative LNAPL displacement and frost penetration for each freeze-thaw cycle.

To evaluate whether the observed displacement is due to increased capillarity due to decreasing temperature or suction induced at the commencement of phase change in the water (freezing), a simple test was performed in the laboratory involving the use of 1 mm diameter capillary tube. In this test, the capillary tube was mounted in a glass beaker and placed inside the environmental chamber and cooled to -2°C from initial room temperature of +19°C. The test results showed that there was an increase in the capillarity height in the system as the temperature decreases. However, the change in capillary height was 4 mm for a 1mm diameter capillary tube. Thus, for the dimension of the freezing cell used in this study, the change in capillarity due to decreasing temperature was relatively small compared with the freezing-induced suction.

The implication of upward mobility of the LNAPL at the commencement of the freezing process is that greater LNAPL accumulation will occur at the start of winter period. The amount of LNAPL will be enhanced by decreased groundwater elevation in the winter period as observed by Iwakun et al. (2008a; and 2010). Upon removal of the accumulated LNAPL, there may be little to no recharge from the formation because the driving mechanisms are discontinuous. However, as winter ends, and spring brings warmer temperature, the accumulable LNAPL in the monitoring well may not be of the same magnitude as that observed during the winter period. Reasons for these may be one or combinations of the following:

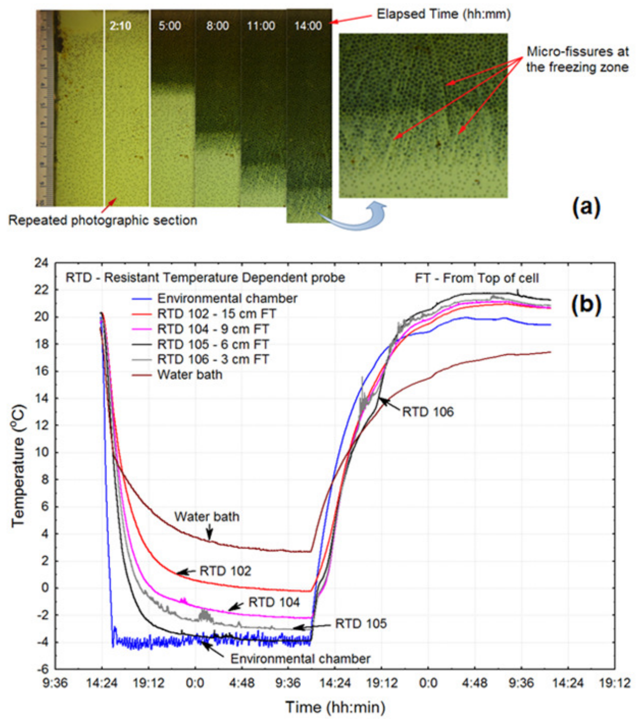

Figure 7 Profile of thermal propagation for freezing test using soluble oil: (a) Snapshots of the observed progressive cryogenic expulsion; (b) temperature profile for the test.

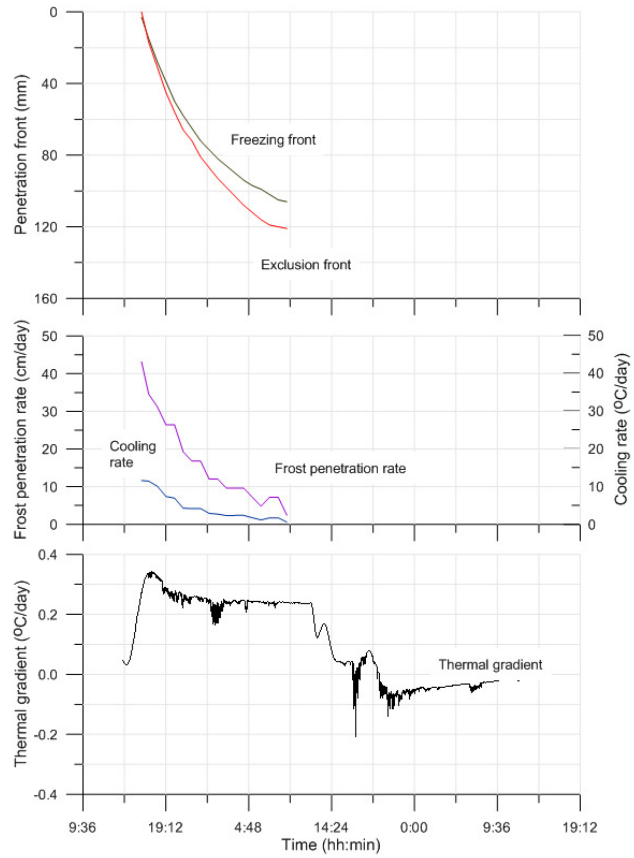

Figure 8 Condensed plot showing the freezing and exclusion fronts, thermal propagation rates and the thermal gradient.

- Elevation of the groundwater table in early spring as winter ends due to snowmelt and precipitation may cause trapping of released LNAPL below the water table.
- The released LNAPL due to thawing are pushed back into the formation by the rising groundwater table, and may be locked-up in localized fissures that are hydraulically disconnected from the main interconnected fracture network when dealing with fractured media.
- Increase in water elevation may enhance downgradient migration of the released LNAPL, thereby reducing the accumulable LNAPL in the monitoring well.

Thus, remobilization of the LNAPL in the formation may result from freezing induced displacement associated with the winter period coupled with decreased groundwater elevation due to little to no precipitation and water consumption.

The results of using Mobilcut-102 soluble oil for the test are summarized in Figures 7 and 8. Mixing was done at 12.5% volume ratio to emphasize visual contrast during analysis because the color of the oil is akin to the color of the fluorescein-water when frozen. The results showed progressive exclusion of the soluble oil forward of the freezing front as shown in Figure 7, and in agreement with previous studies i.e., Konrad and Seto (1991), Chuvilin et al. (2001a and 2001b). The thickness of the excluded oil increased from 0 to 15 mm as freezing progressed downward in the cell. After eight hours, micro-fissures development was observed around the freezing front and the exclusion occurred as fingering as shown in Figure 7a.

The cooling rate at steady state varied from 1.7 to 0.6°C/day as shown in Figure 8, and below the reported value of 4±1°C/day in literature (i.e., Konrad and Seto, 1991) for the optimum occurrence of cryogenic expulsion. Mixing of the soluble oil at 2% volume ratio produced similar results with a thin film of excluded oil below the freezing front. In addition to Mobilcut-102 soluble oil, slightly denser soluble oil named “BAND-ADE® Sawing Fluid” was used with a specific gravity of 1.02 (Table 1). The results are similar to that of Mobilcut-102.

To evaluate the possibility of fissure development in the absence of oil, a new freezing cell was setup and subjected to prolonged continuous freezing. After four days, there were visible micro-fissures in the freezing cell (Figure 9).

This agrees with the statement of Yershov et al. (1988) that there is a natural tendency for micro-fissures development in frozen media and reinforces conclusions from previous studies (i.e., Biggar et al., 1998; and Chuvilin and Miklyaeva, 2003) that the developed micro-fissures are potential pathway for contaminant propagation in frozen media.

The processes discussed above were physical processes, thus, reversible. Another reversible physical process is regelation phenomenon in ice, which involves pressure melting at the interface and refreezing with pressure relief.

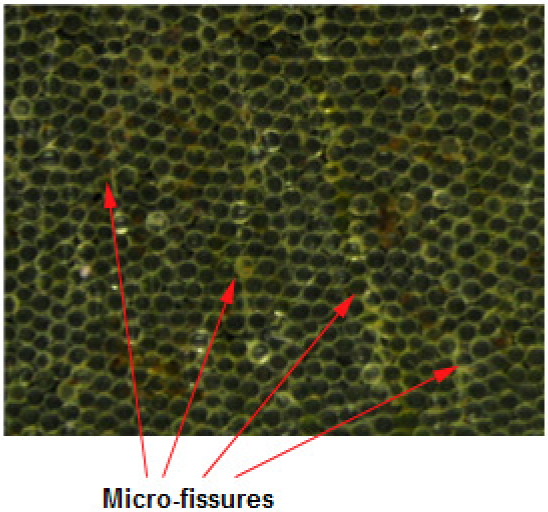

Figure 9 Snapshots of the observed micro-fissures in freezing test from a freezing cell under prolonged freezing with fluorescein-water only.

According to Miller et al. (1975), continuous mobile liquid phase will allow transport from regelation of pore ice. In an unfrozen porous and fractured media, the pressure balance on the LNAPL can be written as follows (Hardisty et al., 1998):

$$h_L \rho_L g = h_{L-W} \rho_w g + \left(\frac{2\sigma \cos\phi}{b} \right) \qquad [3]$$

Where h_L and h_{L-W} are the height of the LNAPL above and below the water table respectively. The LNAPL density is ρ_L, b is the aperture width and ϕ is the contact angle. According to Hardisty et al. (1998), a one meter head of LNAPL will penetrate fracture as small as 10 µm.

However, when dealing with ice in frozen media, the relevant equation is:

$$\begin{aligned} h_L \rho_L g &= h_{L-W} \rho_w g + \left(\frac{2\sigma \cos\phi}{b} \right) + \Delta P_{ice} \\ &= h_{L-W} \rho_w g + \left(\frac{2\sigma \cos\phi}{b} \right) + \frac{L \Delta T}{T \Delta V_w} \end{aligned} \qquad [4]$$

Where ΔV_w is the specific volume change and ΔP_{ice} is the pressure required to melt ice from Clausius Clapeyron equation. The ΔP_{ice} term is often large in the range of 13 MPa per temperature change below freezing. Thus for regelation to be a significant mechanism in LNAPL transport below freezing, the pressure head on the ice would have to be large. Moreover, given that the LNAPL will insulate the ice layer and heat exchange from fresh spill will increase the temperature of the ice, which may lead to melting thereby enhancing downward migration of the LNAPL. However, more studies are needed to know the extent of fissure inducement due to bulk hydrocarbon in a frozen media.

4 CONCLUSIONS

The findings in this study showed that freezing-induced displacement is a viable mechanism contributing to LNAPL migration and accumulation in a permafrost environment. Upward LNAPL remobilization was observed at the commencement of freezing and during thawing. The thermal induced suction was attributed to the upward displacement of LNAPL for the top-down freezing experiment. During thawing, pressure relief coupled with the buoyant nature of the LNAPL enhanced upward remobilization. Test results using soluble oil showed progressive cryogenic expulsion forward of freezing front and corroborated previous studies by Konrad and Seto (1991). Furthermore, developments of micro-fissures were observed in the ice formed within the freezing cell under prolonged freezing and at the freezing front region when soluble oil was used. This reinforces previous assertions by Biggar et al. (1998) and Chuvilin and Miklyaeva (2003) that the micro-fissures developed in freezing media are potential pathway for LNAPL propagation in frozen media.

ACKNOWLEDGEMENT

This study was sponsored by Program for Energy Research and Development (PERD), Natural Sciences and Engineering Research Council (NSERC) of Canada, and Indian and Northern Affairs Canada. Steve Gamble and Christine Hereygers of Geotechnical Center at the University of Alberta, Canada, provided invaluable laboratory assistance from concept to system-setup. Technical inputs by Todd Carter on the fabrication of the freezing cell from the Department of Chemistry at the University of Alberta are greatly appreciated.

REFERENCES

Andersand, O.B., Wiggert, D.C., Davies, S.H., 1996. Frozen soil subsurface barriers: formation and ice erosion. Journal of Contaminant Hydrology, 23:133-147.

Aral, M.M., Liao, B., 2002. Effect of groundwater table fluctuations on LNAPL thickness in monitoring wells. Environmental Geology 45:151-161.

Arenson, L.U., Sego, D.C., 2006. The effect of salinity on the freezing of coarse grained sands. Canadian Geotechnical Journal, 43:325-337.

Barnes, D. L., Chuvlin, E., 2009. Migration of petroleum in permafrost-affected regions. Permafrost soils, R. Margesin (Ed). Soil biology, 16: 263–278. Springer, Germany.

Barnes, D.L., Wolfe, S.M., 2008. Influence of ice on the infiltration of petroleum into frozen coarse grain soil. Petroleum Science Technology, 26:856–867.

Barnes, D.L., Wolfe, S.M., Filler, D.M., 2004. Equilibrium distribution of petroleum hydrocarbons in freezing ground. Polar Record, 40:245–251.

Biggar, K. W., Haidar, S., Nahir, M., Jarrett, P.M., 1998. Site investigations of fuel spill migration into permafrost. Journal of Cold Regions Engineering, 12:84–104.

Biggar, K.W., Neufeld, J.C.R., 1996. Vertical migration of diesel into silty sand subject to cyclic freeze-thaw. In: Carlson, R. (editor). Proceedings of the Eighth International Conference on Cold Regions Engineering. Fairbanks: American Society of Civil Engineers: pp 116–127.

Catalan, L. J. J., Dullien, F.A.L., 1995. Application of gravity drainage to the recovery of residual LNAPL in homogeneous and lensed sand packs. Journal of contaminant Hydrogeology, 18: 279-306.

Chuvilin, E.M., Miklyaeva, E. S., 2003. Investigation of the influence of salinity and cryogenic structure in the dispersion of oil and oil products in frozen soils. Cold Regions Science and Technology, 37: 89-95.

Chuvilin, E.M., Naletova, N.S., Miklyaeva, E.C., Kozlova, E.V., Instanes, A., 2001. Factors affecting spreadability and transportation of oil in regions of frozen ground. Polar Record, 37:229–238.

Ding, M., Kantzas, A., 2007. Capillary number correlations for gas-liquid systems. Journal of Canadian Petroleum Technology, 46(2):27-32.

Dobson, R., Scroth, M.H., Zeyer, J., 2007. Effect of water table fluctuation on dissolution of a multi-component light nonaqueous phase liquid. Journal of Contaminant Hydrogeology 94: 235-248.

Ershov, E. D., Lebedenko, Yu, P. Chuvilin, E.M., Naumova, N.S., (1992. Mass transfer in freezing saline soils'. First International Conference Oil Pedology, Pushchino, Russia, pp: 115-122

Frolov, A.D., 1982. Physical model of frozen rocks. wIzvestiia vysshikh uchebnykh zavedeniix Geologiia irazvedka, 11: 134–141, Nov. Žin Russian.

Grant, S.A., Bachmann, J., 2002. Effect of temperature on capillary pressure. In: Environmental Mechanics, Water, Mass and Energy Transfer in the Biosphere (Raats, P.A.C., D.E. Smiles, and A.W. Warrick, Eds.) Geophysical Monograph Series, v. 129. Washington, DC: American Geophysical Union, 199-212. (ERDC/CRREL MP-02-5905)

Hardisty, P. E., Wheater, H. S., Johnston, P. M., Bracken, R. A., 1998. Behavior of Light Immiscible Liquid Contaminants in Fractured Aquifers. Geotechnique, 48(6):747–760.

Iwakun, O., and Biggar, K., 2007. Behavior of spilled petroleum hydrocarbon at Colomac mine site, NWT. Proceedings of 60th Canadian Geotechnical Conference and the 8th Joint CGS/IAH-CNC Groundwater Conference, Ottawa, pp 2106-2114.

Iwakun, O., Biggar, K., Sego, D., 2008b. Influence of temperature and groundwater fluctuation on LNAPL migration at Colomac mine site. Proceedings of Ninth international conference on permafrost, edited by Kaine, D. L., and Hinkel, K. M., 1:815-820.

Iwakun, O., Biggar, K., Van Stempvoort, D., Bickerton, G., Voralek, J., 2008a. Fuel contamination characterization in permafrost fractured bedrock at the Colomac mine site, NWT. Cold Region Science and Technology, 53(1): 56-74.

Iwakun, O., Biggar, K.W., Sego, D., 2010. Estimation of actual LNAPL thickness in a fuel-contaminated mine site. Cold Region Science and Technology, 60:212-220.

Konrad, J.M., McCammon, A.W. , 1990. Solute partitioning in freezing soils. Canadian Geotechnical Journal, 27(6): 726-736.

Konrad, J.M., Seto, J. T. C., 1991. Freezing of a clayey silt contaminated with an organic solvent. Journal of Contaminant Hydrology, 8 (3–4): 335–356.

Lenhard, R.J., Johnson, T.G., Parker, J.C., 1993. Experimental observations of nonaqueous-phase liquid subsurface movement Journal of Contaminant Hydrology, 12: 79-101.

Miller, R.D., Loch, J.P.G., Breseler, E., 1975. Transport of water and heat in a frozen permeameter. Soil Science Society of America Journal, 39(6): 1029-1036.

Niven, R.K., Singh, K., 2008. Mobilization and rupture of LNAPL ganglia during freeze-thaw: Two dimensional cell experiments. Environmental Science Technology, 42(15):5467-5472.

Panday, S., Corapcioglu, M.Y., (1991. 'Solute rejection in freezing soils,' Water Resources Research, 27(1): 99-108.

Ryan, R., Dhir, V.K., 1993. The Effect of Soil Particle Size on Hydrocarbon Entrapment Near a Dynamic Water Table. Journal of Soil Contamination, 2(1): 59-90, 1993.

Ryan, R.G., Dhir, V.K., 1996. The effect of interfacial tension on hydrocarbon entrapment and mobilization near a dynamic water table. Journal of Soil Contamination, 5(1):9-34.

Tumeo, M.A., Davidson, B., 1993. Hydrocarbon exclusion from ground water during freezing. Journal of Environmental Engineering-Asce, 119(4): 715-724.

Wilson, D.G., Mackay, D., 1987. The behavior of oil in freezing situations. Unpublished report of Environmental Protection Directorate, River Road Environmental Technology, Ottawa. 78p

Yershov, E.D., Lebedenko, Yu.P., Chuvilin, E.M., Yazynin, O.M., 1988. Microstructure of frozen soils. In: Yershov, E.D. (Ed.), Moscow State University, Moscow, p. 186. In Russian.